Laser-induced multiple ionization of molecular ion beams: N_2^+, CO^+, NO^+, and O_2^+

B. Gaire, J. McKenna, Nora G. Johnson, A. M. Sayler, E. Parke, K. D. Carnes, and I. Ben-Itzhak

J. R. Macdonald Laboratory, Department of Physics, Kansas State University, Manhattan, Kansas 66506, USA

We have simultaneously measured the kinetic energy release and the angular distributions for the multiply charged fragmentation of diatomic molecular ions, N_2^+, CO^+, NO^+, and O_2^+, in intense ultrashort laser pulses. Using a coincidence three-dimensional momentum imaging method we unambiguously separate all fragmentation channels, including dissociation, since we measure both neutral and ionic products. Based on the experimental results, we conclude that the fragmentation mechanism that explains the multielectron dissociative ionization of these molecular ions entails a stairstep process. This mechanism, which involves stretching the molecules prior to each sequential ionization step, is similar to that proposed in some earlier studies that use neutral molecules as targets. We find that structure in the breakup of the molecules to lower charge states is molecule specific, while, for breakup to higher charge states, all species tend to follow a universal trend.

I. INTRODUCTION

The multielectron dissociative ionization (MEDI) of diatomic molecules in ultrashort intense laser pulses is an ongoing area of interest as it enables us to better understand laser-driven molecular dynamics. So far a broad range of studies have been carried out on this subject, e.g., [1–7], and various processes have been identified in order to explain the multiple ionization and fragmentation pathways of molecules. These include, for example, direct ionization [8,9], electron rescattering [10], and enhanced ionization [11,12]. We illustrate these processes schematically in Fig. 1 and discuss them in more detail later.

The goal of this work is to explore experimentally the fragmentation mechanism for MEDI of small diatomic molecular ions (N_2^+, CO^+, NO^+, and O_2^+). In contrast to most earlier studies on MEDI that use neutral molecules as precursor targets, we begin with the singly charged molecular ions themselves in the form of an ion-beam target. One of the main reasons we choose to study the more technically challenging ion-beam targets is that history has shown that ion beams can behave differently from their neutral partners, thereby unveiling new dynamics. A few examples include the observation that electron rescattering ionization of Ar^+ is suppressed compared to Ar [13]. Also, H_2^+ [14] dynamics in an intense field are significantly different from those of H_2 [3].

The molecular ion targets are exposed to ultrashort (40 and 7 fs) intense 790 nm laser pulses. We apply a coincidence three-dimensional (3D) momentum imaging method that allows us to detect and separate the charged fragments from the neutrals and also differentiate fragmentation channels from each other [14–16]. The molecular ions under study, N_2^+, CO^+, NO^+, and O_2^+, are representative of many-electron systems. Their constituent atoms are in the same row of the periodic table. At the intensities used here (up to 7×10^{15} W/cm^2) the ionization of more than one electron is probable in the intense laser field, hence, we focus our discussion on multiple ionization.

The possibility of multiple ionization leads to complex behavior of these molecules. Previous studies indicate that multiple ionization can occur either directly [8,9] or indirectly [11,12]. Direct multiple ionization can occur as a vertical transition near the equilibrium internuclear distance R_e through multiphoton absorption or tunneling, or by electron rescattering. On the other hand, indirect multiple ionization occurs at internuclear distances $R > R_e$ following stretching of the molecule in the laser field. Additionally, the indirect ionization process is often believed to occur around some critical distance R_c where ionization is enhanced by charge resonance. We will review these processes briefly as follows:

(i) Direct ionization [8,9]: in this case the molecules are ionized near R_e, i.e., there is very little stretching of the molecule during ionization [see Fig. 1(a)], thus the nuclei can be treated as frozen. If the molecular potentials are more repulsive at smaller R than at large R, as is typically the case for multiply ionized states, the kinetic energy release (KER) will usually be high for this process.

(ii) Electron rescattering [10]: in this process an ionized electron gains energy in the electric field of the laser and returns to the parent ion after typically $\sim 3/4$ of a laser cycle to excite or ionize an additional electron(s). Since the molecule does not have enough time to stretch much during the short time interval before the electron returns [9,17,18] [see Fig. 1(b)], R values for multiple ionization will typically be similar to that of the initial ionization step.

(iii) Charge-resonance enhanced ionization [11,12]: in the past, many measurements were performed under various experimental conditions on neutral molecular targets. One of the main findings of these experiments was that the KER was lower than the Coulomb explosion energy for breakup at R_e. This behavior has been explained in terms of the stretching of molecules prior to ionization. Specifically, a molecule will stretch before ionization such that the electron will localize on one of the two nuclear centers, hence, the ionization will be enhanced once the electron is localized—herein we refer to this process as enhanced ionization. This leads to the ionization of molecules at some R that is greater than R_e and is called the critical internuclear distance R_c [see Fig. 1(c)].

In addition to the processes discussed above, other possible mechanisms for MEDI are (i) the molecules can stretch only on the dissociation curve and then ionize to different levels at $R_e < R < R_c$ [see Fig. 1(d)], and (ii) stretch in each
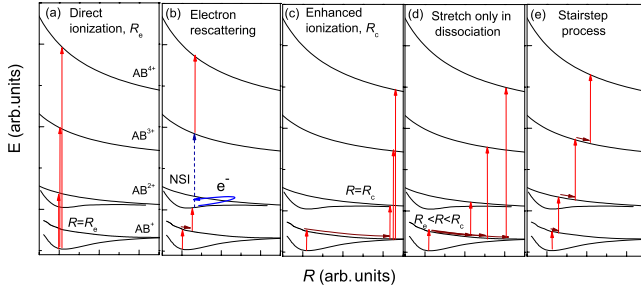
FIG. 1. (Color online) Schematic diagrams illustrating the different mechanisms for the multiple ionization of a typical molecule, AB^+, in an intense laser field (a) direct ionization, (b) electron rescattering (nonsequential ionization, NSI), (c) enhanced ionization, (d) stretch only in dissociation, and (e) stairstep process. For a discussion of the mechanisms refer to the text.

step before further ionization to the next level in a sequential manner at $R_e < R < R_c$ [2,4]. We refer to this latter mechanism, shown in Fig. 1(e), as a stairstep process.

There are several phenomena that are common to each of these MEDI mechanisms discussed above. For example, typically the MEDI of molecules leads to their Coulomb explosion [19–21]. This occurs when the laser field is intense enough that the molecule is ionized to a repulsive potential energy curve (PEC). The PEC is often approximated by a Coulomb potential given by $q_1 q_2 / R$ (in atomic units), where q_1 and q_2 are the atomic charges. The fragments thus repel each other and "explode." By measuring the KER distribution and assuming ionization occurs rapidly, the R dependence of ionization can be retrieved from the measured KER distribution. This is the basic idea for the Coulomb explosion imaging technique [21,22]. That is, if ionization occurs at small R the resulting fragments share high KER, and at large R they share low KER.

Another phenomenon that is common in MEDI is molecular alignment. There are generally two types of alignment to consider, *geometric* and *dynamic* alignment [3,23,24]. Molecules that are aligned at some angle with respect to the electric field of the laser are ionized preferentially over other molecules. This angle-dependent nature of the ionization of molecules is called geometric alignment and is different for each molecule, mainly dependent on the orbital of the valence electrons [25]. However, there is also the possibility that the molecules can align themselves in the presence of the laser field due to the torque exerted by the electric field of the laser. This behavior is called dynamic alignment. As well as aligning during the laser pulse, it has also been shown that the molecules can continue to align after the pulse, a phenomenon referred to as postionization alignment [26,27].

As a follow-up to geometric alignment, molecular Ammosov-Delone-Krainov (MO-ADK) theory [25] was developed. This model predicts the rate and angular dependence of the ionization of molecules based on the shape of the valence electronic cloud. It has been successfully used to explain enhancement and suppression of the ionization rate of some molecules over atoms with similar ionization potential [25].

The molecular ions explored in our study have been investigated previously using intense laser pulses on neutral moleculer targets for decades now. The most common experimental methods that are in use by other groups include time-of-flight (TOF) mass spectrometry [6,24,28–30], covariance mapping [31], mass-resolved momentum imaging [32], cold-target recoil ion momentum spectroscopy [33], and velocity-map imaging [7]. Some of the work has been done at similar wavelength and intensities to those we report here, but with slightly different pulse durations, e.g., for N_2^+ [5–7,22,24,28,29,33–36], for CO^+ [36–38], for NO^+ [30,32,37,39–41], and for O_2^+ [28,35,36]. However, the experimental technique used in the current study is different from these previous studies in the sense that we use a molecular ion-beam target and a coincidence 3D momentum imaging technique that allows us to detect both the neutral and ionic fragments. The obvious benefit of detecting neutral fragments is that we are able to clearly separate by the coincidence measurement the molecular dynamics for dissociation ($AB^+ \rightarrow A^+ + B$ or $A + B^+$), and charge-asymmetric breakup of dications in single ionization (e.g., $AB^+ \rightarrow AB^{2+} + e^- \rightarrow A^{2+} + B + e^-$) from the dynamics of the other channels. Furthermore, a strength of this coincidence 3D momentum imaging technique is that it provides both the KER and the angular distributions of the breakup channels.

Our goal is to present a general picture to explain our experimental observations for all molecular ions studied. We find that fragmentation to higher charge states results in similar KER and angular structure for all species under study, while fragmentation to lower charge states yields quite different distributions except for the isoelectronic molecular ions N_2^+ and CO^+ that are similar in many respects.

II. EXPERIMENTAL SETUP

We have applied a coincidence 3D momentum imaging method that allows us to separate neutral and ionic fragments with different mass-to-charge ratio (m/q) and, hence, distinguish dissociation from ionization and different ionization channels from each other. For example, a coincidence time-of-flight map for the different breakup channels that result from CO^+ fragmentation is shown in Fig. 2. Clearly all the breakup channels are well resolved. The experimental method has been described in our earlier publications [14–16] so here we discuss it only briefly.

The molecular ions are produced in an electron cyclotron resonance ion source by electron impact ionization. These ions are accelerated to 9 keV and guided toward the laser interaction region using static electric and magnetic fields. The ion beam is collimated to about 0.6×0.6 mm using ion optics and a pair of four-jaw slits and is crossed with a laser beam at the interaction region within a longitudinal electrostatic spectrometer. Here, the molecular ions are dissociated or ionized by the ultrashort intense laser pulse. The electric field of the spectrometer then accelerates the fragment ions toward the detector according to their m/q values. The fragments can therefore be distinguished by their time of flight. In addition the transverse component of the breakup energy imparted to the fragments separates the fragments from the primary beam that is collected in a small on-axis Faraday cup (2 mm in diameter). Fragments with low KER
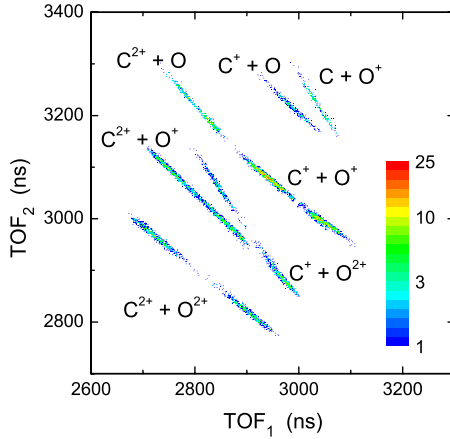
FIG. 2. (Color online) Coincidence TOF density plot showing the TOF of the particle with the smaller m/q value to hit the detector (TOF_1) against that of the particle with the larger m/q value (TOF_2), from the fragmentation of CO^+ in 40 fs, 7×10^{15} W/cm^2 pulses. We plot the data after momentum conservation in order to present only true two-body breakup events. The plot shows that all the breakup channels observed in our measurement are clearly distinguished from each other, including those involving a neutral fragment.

(<0.1 eV) are lost due to blocking by the Faraday cup. The majority of fragments, however, hit a microchannel plate detector with a delay-line anode position readout. From the position and time-of-flight information of coincident fragments, recorded in event mode, the complete three-dimensional kinematics of the heavy fragments are computed, i.e., the KER and the angular distribution, $\cos \theta$, where θ is the angle between the laser polarization and the molecular dissociation axis. Note that we do not detect the electrons in our measurements.

The laser used in the experiment is a Ti:sapphire system (790 nm), providing linearly polarized 40 fs (full width at half maximum in intensity, FWHM) pulses at 1 kHz repetition rate. To achieve ~7 fs duration, the laser pulses are compressed using a neon-filled hollow-core fiber and chirped mirror arrangement [42]. The pulses are characterized using frequency-resolved optical gating [43]. The pulses are transported to, and then focused onto, the ion-beam target using an $f=203$ mm off-axis parabolic mirror. The laser intensity at the target is varied by using a technique known as an intensity selective scan [44,45].

III. RESULTS AND DISCUSSION

We have measured the KER and the angular distributions for the different breakup channels of N_2^+, CO^+, NO^+, and O_2^+ using 40 and 7 fs, 790 nm laser pulses for several intensities up to 7×10^{15} W/cm^2. For simplicity we only present a selection of this data, but further results can be communicated upon request. In general, fragmentation channels are referred to as (q_1, q_2), where q_1 and q_2 are the charges of the less and more massive fragments, respectively. For example, double ionization of CO^+ leading to $C^+ + O^{2+}$ is referred to as the (1,2) channel.

A. Long pulse: 40 fs

We start our discussion with the results for 40 fs pulses, since we have observed more channels at this pulse duration compared to 7 fs pulses at the same intensity. The data at 7×10^{15} W/cm^2 are presented in Fig. 3 as KER-cos θ density plots in the upper panels [(a)–(d)] and KER distributions in the lower panels (e). By surveying the spectra shown in Fig. 3 as a whole, we can make a few general statements. First, comparing dissociation [Fig. 3 (i)] between the different molecules, the spectra look quite different for each of the species with the exception of N_2^+ and CO^+. All molecules display structure in their KER distributions, pronounced in the one-dimensional (1D) KER plots [see panel (i), (e)]. Second, in single ionization [Fig. 3 (ii)] some aspects of the spectra are remarkably similar such as the angular distributions showing a narrowly aligned ridge with a broader angular base. Other aspects, however, look very different as exemplified by the different structures in KER. Finally, in multiple ionization [Fig. 3, (iii) and (iv)] the molecules lose this structure in KER and start to resemble one another more closely both in angle and KER shape. We will review each of these fragmentation channels in turn and posit an explanation for the features observed.

1. Dissociation

The dissociation of N_2^+ (1,0) and CO^+ (1,0) and (0,1) look qualitatively similar. Both molecules display a low-KER peak around 1 eV and a weaker high-KER peak around 6 eV [shown in the inset of Fig. 3(e), (i)]. This double peak behavior is reminiscent of our earlier measurements for N_2^+ with ~7 fs pulses [46]. There we identified the low-KER peak as arising from dissociation via low-lying electronic states that are shallow in potential energy (similar to observations by other groups [6,29,34]). In contrast, the high-KER peak was an observed feature coming from excitation of an inner-shell electron ($2\sigma_g$) leading to dissociation on steep high-lying electronic states. We believe the same mechanisms are valid for the 40 fs pulses used here. Since N_2^+ and CO^+ ground states have the same electronic configurations, i.e., $1\sigma_g^2 1\sigma_u^2 2\sigma_g^2 2\sigma_u^2 1\pi_u^4 3\sigma_g^1$ for N_2^+, which is equivalent to $1\sigma^2 2\sigma^2 3\sigma^2 4\sigma^2 1\pi^4 5\sigma^1$ for CO^+, it is reasonable to expect that the equivalent inner-shell electron gets excited in CO^+ leading to its observed likeness with N_2^+.

Neither O_2^+ nor NO^+ display the high-KER peak observed in N_2^+ and CO^+. Nonetheless, O_2^+ is rich in other structure displaying multiple low-KER peaks below ~3 eV. We previously studied dissociation of O_2^+ at lower intensities [47], and there we outlined a method for determining the important dissociation pathways. As the structure in the present experiment looks similar to that in our previous experiment, details of the electronic states involved in O_2^+ dissociation may be found in our earlier publication [47]. The important point in this context is that the presence of structure in O_2^+ reflects the multitude of electronic states that can be accessed by the laser, giving many dissociation pathways. Thus, it seems that the dissociation spectra are dictated strongly by the individual nature of a molecule's electronic potentials, hence the reason why the various parent molecular species each behave differently.
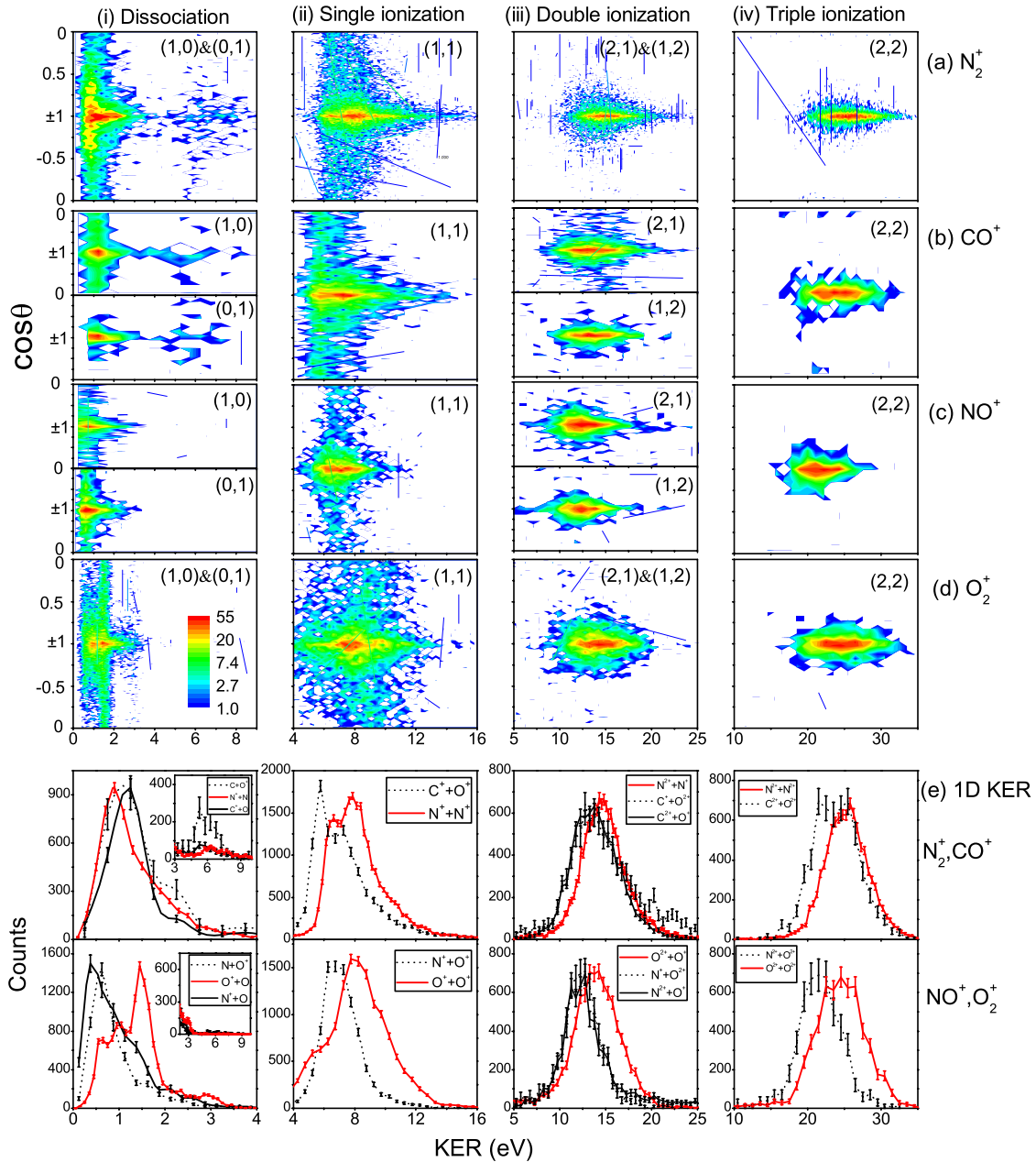
FIG. 3. (Color online) The KER and angular distributions of the different fragmentation channels [(i) dissociation (1,0) and (0,1), (ii) single ionization (1,1), (iii) double ionization (2,1) and (1,2), and (iv) triple ionization (2,2)] of N_2^+, CO^+, NO^+, and O_2^+ for 40 fs, 7×10^{15} W/cm^2 pulses. The upper panels [(a)–(d)] are KER-cos θ plots with the same cos θ scale and the lower panels (e) are 1D KER plots integrated for all angles. The error bars denote the statistical uncertainty in the data. The color scale is the same for all the density plots.

This assessment is supported by the angular distributions in Fig. 3 (i). Generally, the type of the dissociative transition is determined by the change in the angular momentum quantum number $\Delta\Lambda$ of the states involved [47,48]. A parallel transition corresponds to $\Delta\Lambda=0$ (e.g., $\Sigma \leftrightarrow \Sigma$), leading to a $\cos^n \theta$ distribution, where n is the number of photons involved. A perpendicular transition corresponds to $\Delta\Lambda= \pm 1$ (e.g., $\Sigma \leftrightarrow \Pi$), giving a $\sin^n \theta$ distribution. The plots in Fig. 3 show that, for all molecules, one observes counts for both cos $\theta=0$ and cos $\theta= \pm 1$ indicating the presence of both perpendicular and parallel transitions, respectively, with the parallel transitions dominating. The fact that both types of transitions are observed (and for some peaks a mixture of both)

shows that the dissociation spectra are influenced by the individual nature of the molecules' electronic states, i.e., their angular momentum quantum number. Thus, the observed angular distribution will be specific to a particular dissociation path of the molecule.

2. Single ionization

Regarding single ionization leading to the (1,1) channel [Fig. 3 (ii)], the angular distributions of the different molecules in some respects appear similar, each showing a dominant aligned feature with a much broader angular base. The reason for the observed shape of these distributions, how-
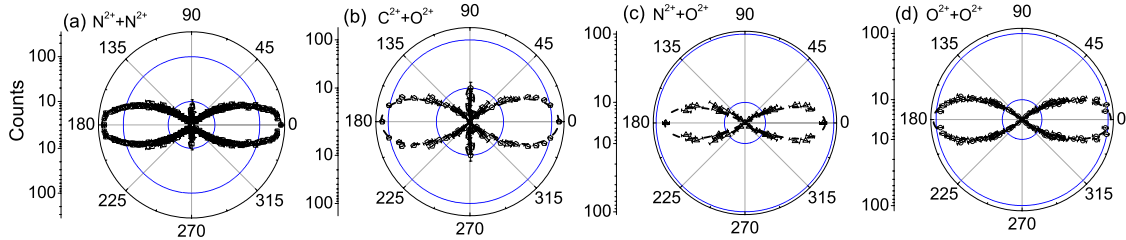
FIG. 4. (Color online) Measured angular distributions (plotted on a log scale) for triple ionization (2,2) of (a) N_2^+ (fitted function $a\cos^{24}\theta + b\sin^{24}\theta$), (b) CO^+ (fitted function $a\cos^{18}\theta + b\sin^{30}\theta$), (c) NO^+ (fitted function $a\cos^{18}\theta$), and (d) O_2^+ (fitted function $a\cos^{18}\theta$), using 40 fs, 7×10^{15} W/cm^2 pulses, integrated for all KER. The dotted lines are fitted functions. The error bars denote the statistical uncertainty in the data. The lower half of the data is mirrored from the upper half.

ever, can be complicated by several factors. MO-ADK predicts that in the tunneling regime the angular distribution for the (1,1) channel should reflect the symmetry of the orbital of the most loosely bound electron of the molecule [25]. For example, for the N_2^+ $X^2\Sigma_g^+$ ground state $(…1\pi_u^4 3\sigma_g^1)$ the outermost electron is in a σ_g orbital and ionization should be peaked along the laser polarization. For the O_2^+ $X^2\Pi_g$ ground state $(…3\sigma_g^2 1\pi_u^4 1\pi_g^1)$, where the outer electron is in a π_g orbital, ionization is predicted to peak at $\sim40°$ to the laser polarization [33]. However, this only works well at relatively low intensities. As described by Voss et al. [33], at high intensities deep into the sequential ionization regime as used here $(7\times10^{15}$ W/cm$^2)$, the angular distribution will be influenced by other steps involved in the ionization process such as intermediate excitation processes. Indeed, Voss et al. observe a transition in the angular distribution of the O_2^+ (1,1) channel changing from peaking near 40° at 10^{14} W/cm^2 to strongly peaking at 0° at 10^{15} W/cm^2 (for 7 fs pulses). The spectra we observe at 7×10^{15} W/cm^2 in Fig. 3 seem to agree with this alignment effect, since the dominant contribution to single ionization is strongly aligned for all molecules, irrespective of the initial electron orbital. This may also, at least partly, be due to dynamic alignment [23] where molecules rotate their internuclear axis toward the laser polarization during the pulse or even after the pulse [26,27]. This is supported by comparison with 7 fs pulses (that we discuss later), which display a lower degree of alignment because of less rotation time in the field.

The fact that all molecules show some perpendicular fragmentation for the (1,1) channel is perhaps an indication that the ionization process proceeds in a stepwise manner. Initially the singly charged molecular ion is excited to a dissociative state, which is then ionized. In this way the (1,1) channel should reflect some of the characteristics of the (1,0) and (0,1) dissociation channels. This is indeed the case as is evident in Fig. 3 since the angular distributions for dissociation and single ionization spectra are qualitatively similar, both displaying a dominant sharply aligned feature with a broader angular base.

Further evidence for this stepwise process is found in the KER distributions. If ionization does follow on from an initial dissociative-excitation step, we might expect the structure observed in dissociation to transfer also to the (1,1) channel. We appear to observe this behavior in Fig. 3. Both N_2^+ and CO^+, which show low- and high-KER peaks in the (1,0) and (0,1) channels, also show a double peak structure

for the (1,1) channel. The reason the energy separation of the (1,1) peaks is smaller than for (1,0) or (0,1) is simply because only part of the dissociation KER is imparted to the fragments before ionization occurs. On the other hand, NO^+, which only has a single low-KER peak for (1,0) and (0,1), has a single peak for the (1,1) channel. Likewise, O_2^+, which has multiple (1,0) peaks, shows a structured (1,1) KER distribution, which although not well resolved, could be explained by the presence of several peaks arising from the dissociation step. Viewed overall, there are some remarkable similarities between the (1,1) and the (1,0) and (0,1) channels. Thus, the KER peaks in the (1,1) channels can qualitatively be linked to the peaks in the (1,0) and (0,1) channels.

As an aside, we do note that we also observe the single ionization charge-asymmetric (2,0) channel for each of the molecules (not shown). This channel is considerably weaker than the symmetric (1,1) channel [typically $<10\%$ of the (1,1) yield] and has a higher appearance intensity. This is explained by the fact that the (2,0) fragmentation limits are between 11 eV (for CO^+) and 21 eV (for O_2^+) higher than the (1,1) limit. We do not observe the corresponding (0,2) channel for CO^+ and NO^+ as this limit is a further 13 eV (for CO^+) and 4.5 eV (for NO^+) higher than the (2,0) limit. Also, the KER for the (2,0) channel is considerably lower than for the (1,1) channels [on average KER ~3 eV for (2,0) compared to KER ~7 eV for (1,1)]. Qualitatively, the Coulomb repulsion between the (1,1) charged centers will lead to higher KER.

3. Multiple ionization

In Fig. 3, the multiple ionization [double (iii) and triple (iv)] of all the molecular ions under study looks roughly similar. Their angular distributions are all quite strongly peaked along the laser polarization, with the exception of the N_2^+ and CO^+ (2,2) channels that have a weak perpendicular component (see Fig. 4, to be discussed later). Similarly, their KER distributions look alike, all molecules showing a single broad peak for the (2,1), (1,2), and (2,2) channels. The only major differences are the KER values, which differ from molecule to molecule by up to 3 eV and 5 eV for double and triple ionization, respectively, and the KER widths which vary by a few eV. The similarity of the different molecules suggests that their electronic structure is less important for multiple ionization. More specifically, the transient multiply charged molecular states, e.g., CO^{3+} and CO^{4+}, become Coulomb-like $(q_1 q_2/R)$ for stretched R [49], giving a first
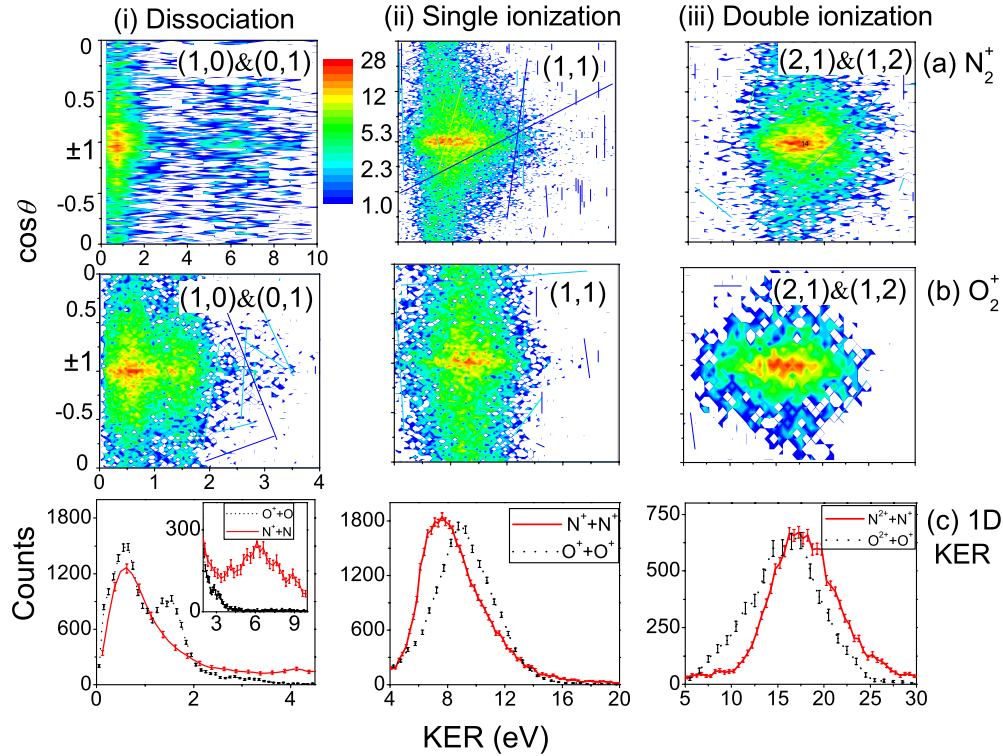
FIG. 5. (Color online) Same as Fig. 3 for N_2^+ and O_2^+ but for 7 fs, 7×10^{15} W/cm^2 pulses. Note that (2,1) was the highest fragmentation channel observed for 7 fs. The error bars denote the statistical uncertainty in the data. The color scale is the same for all the density plots.

indication that the molecules stretch en route to ionization in these channels. Thus, at stretched R the electronic states of all molecules resemble one another.

Based on our experimental results, we believe that the mechanism for multiple ionization can be explained using a stairstep picture, shown in Fig. 1(e), that is similar to the mechanism used in some earlier studies to explain MEDI of neutral molecules [2]. First, though, we rule out other possible mechanisms.

Previously, under certain conditions, a common mechanism suggested for multiple ionization was electron rescattering [9,10,17]. This occurs when a linearly polarized laser field drives an initially ionized electron back to recollide with its parent molecular ion causing ionization, or excitation followed by field ionization, of a secondary (or more) electron(s). A common test to check if this process occurs is to use circularly polarized light, whereby the returning electron misses the parent ion due to a large transverse spread in momentum [10]. To normalize the peak laser field strength one must compare linearly polarized light at half the power of the circularly polarized light. Consequently, we have compared linearly polarized pulses at 3.5×10^{15} W/cm^2 with circularly polarized pulses at 7×10^{15} W/cm^2 and find no significant reduction in the multiple ionization yield for the circular polarization. Since electron rescattering becomes an even smaller effect at higher intensity (because higher intensity is further into the sequential ionization regime), we conclude that rescattering plays no major role for the spectra shown in Fig. 3 at 7×10^{15} W/cm^2.

In a similar way that electron rescattering typically occurs within a few femtoseconds of initial ionization, if we use

sufficiently short pulses multiple ionization will also occur rapidly. If this is the case, the molecule does not have much time to stretch between ionization stages, thus ionization is "direct." That is, it is approximately a vertical transition for which $R \sim R_e$. Since the multiply charged molecular states are almost Coulomb-like, ionization at R_e will lead to large KER from the Coulomb explosion of the fragments. For example, for double ionization of N_2^+ to the (2,1) channel, direct ionization from $R_e = 2.13$ a.u. would give KER $= 25.5$ eV. The observed KER for N_2^+ (2,1) is centered at 14 eV, which is much lower. This suggests that direct ionization does not occur for these 40 fs pulses. Even using 7 fs pulses (see Fig. 5) the KER is centered at only 17 eV which is still much lower than for direct ionization.

In contrast to direct ionization, it has been suggested that molecules stretch on their dissociation potentials before ionizing [11,12]. In particular, there is a predicted critical internuclear distance R_c where ionization is enhanced due to the electron getting localized on one of the two charged centers prior to being ionized. We have calculated R_c for all the species used in the current study using a classical model outlined in Ref. [4]. We find that the R_c value for the lowest ionization channels of N_2^+ is roughly ~ 7.0 a.u., in agreement with the values in Refs. [4,6,50]. For CO$^+$ it is about 6.5–8.2 a.u., for NO$^+$ it is about 6.1–7.3 a.u., and for O_2^+ it is about 5.8–7.5 a.u.. Using the least extreme case, O_2^+, as an example, ionization on the (2,1) channel at $R = 5.8$ a.u. would give an energy release of ~ 9.4 eV, assuming a Coulomb potential. This, added to about 2 eV or less from dissociation, would give a KER value of just over 11 eV. Since the observed centroid for O_2^+ (2,1) is 14 eV, this indicates

that the molecules do not stretch on the dissociation curve or on the parent molecular ion PEC as far as R_c before ionizing. The other molecular ions follow the same behavior.

Having ruled out electron rescattering, direct ionization at R_e, and enhanced multiple ionization at R_c as mechanisms to explain multiple ionization, there only remain a couple of options: (i) stretching only on the dissociation curve followed by ionization at $R_e < R < R_c$ [Fig. 1(d)], or (ii) stretch and ionize, sequentially, in a stairstep process as illustrated in Fig. 1(e).

Option (i) seems unlikely on several grounds. First, if all the ionization stages were preceded directly by dissociation, one might expect that the dissociation structure would be reflected in all the multiple ionization channels. Figure 3 shows that this is not the case and that only the (1,1) channel shows any resemblance to dissociation. Second, by stretching only on the dissociation states, bridging the large energy gap to the high-lying multiple ionization states would seemingly require a much higher intensity than if one electron was stripped off at a time.

In view of these findings we are left with the stairstep process where the molecule first stretches on the (1,0) channel [or (0,1)], then ionizes, followed by stretching on the (1,1) channel, then ionizing again, and so on, i.e., sequential ionization. The data in Fig. 3 appear consistent with this mechanism. Since each subsequent ionization step occurs later in the pulse, the laser field has more time (and intensity) to populate a broad higher rotational J distribution which leads to the angular distributions gradually becoming more aligned for the higher ionization stages, (however, see note in Ref. [51]). Also, any structure in the KER that was present in the initial dissociative step gradually gets washed out over the course of the later ionization steps.

Using the change in KER from one ionization stage to the next we can get an estimate of the R values at which the ionization steps occurred by using an expression, $\text{KER}_{(q_1,q_2)} = \text{KER}_{(q_1,q_2-1)} + \frac{q_1 q_2}{R_{(q_1,q_2)}} - \frac{q_1(q_2-1)}{R_{(q_1,q_2)}}$. For example, for N_2^+ multiple ionization we find that ionization to (2,2) occurs at $R \sim 4.9$ a.u. while for (2,1) it occurs at $R \sim 3.9$ a.u. Our previous study [46] of N_2^+ showed that single ionization to (1,1) occurs for $R = 2.5$–3.0 a.u., while dissociation begins near $R = 2.0$ a.u. Thus, overall we can build up a picture of the fragmentation process.

Briefly, we return to discuss the angular distributions of the (2,2) channels shown in Fig. 4 as polar plots. While by far the dominant (2,2) contribution is strongly peaked along the laser polarization ($\sim \cos^{18} \theta$ to $\cos^{24} \theta$), intriguingly for N_2^+ and CO^+ we observe weak side lobes showing perpendicular contributions that are absent for O_2^+ and NO^+. This suggests that some specific molecular orbital transitions (e.g., $\pi \rightarrow \sigma$) are involved, a similar phenomenon to that observed for the (3,1) and (3,2) channels starting from N_2 [7]. The presence of similar side lobes for N_2^+ and CO^+ is understandable as these molecules are electron similar, while they differ from O_2^+ and NO^+. Thus, while we have found that the angular distributions for multiple ionization are dominated by dynamic alignment, there is some evidence to suggest that geometric alignment also plays a role.
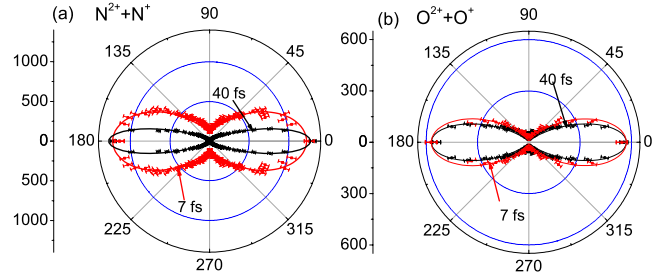

FIG. 6. (Color online) Angular distributions for the double ionization [channel (2,1)] of (a) N_2^+ (fitted functions $a \cos^4 \theta + b \sin^2 \theta$ for 7 fs and $a \cos^{24} \theta$ for 40 fs are denoted by lines) and (b) O_2^+ (fitted functions $a \cos^6 \theta + b \sin^2 \theta$ for 7 fs and $a \cos^{10} \theta + b \sin^2 \theta$ for 40 fs are denoted by lines) 7×10^{15} W/cm² pulses. The error bars denote the statistical uncertainty in the data. The lower half of the distribution is mirrored from the upper half.

B. Short pulse: 7 fs

As a test of some of the conclusions we have come to based on our 40 fs data, we repeated the measurements for the same molecular ions using 7 fs pulses. Since the comparative trends between molecules are similar in this case, for simplicity we display only the results for N_2^+ and O_2^+ in Fig. 5. As before the KER-cos θ density plots and the 1D KER plots are presented.

The first point to note is that for the 7 fs pulses of the same peak intensity fewer fragmentation channels are observed, i.e., (2,1) is the highest fragmentation channel. This is consistent with the stairstep fragmentation mechanism. For shorter pulses, the molecules have less time to stretch between ionization steps. Thus, ionization occurs at smaller R values where the energy gaps between ionization stages are larger making it harder to ionize by multiphoton absorption. This also explains why in general the KER is larger for the 7 fs pulses. For example, for the N_2^+ (2,1) channel the KER is 17 eV for 7 fs compared to 14 eV for 40 fs. At smaller R, ionization projects the molecular wave packet onto a higher-lying part of the final electronic potential leading to higher KER of the fragments.

Another interesting point is that for O_2^+ dissociation (1,0), the structure in the spectra differs quite dramatically compared to 40 fs (Fig. 3). This agrees with the conviction that the features of the dissociation spectra are predominantly determined by the molecular wave packet dynamics on the electronic potentials specific to that molecular ion. For 40 fs there is ample time for the O_2^+ molecule to stretch between crossings of different dissociation pathways. However, for 7 fs dissociation is mostly limited to direct excitation from the initial O_2^+ state since the molecule does not have enough time to expand. Thus, large differences between long and short pulses are anticipated and observed.

Comparing the 7 and 40 fs angular distributions for multiple ionization to the (2,1) channel of N_2^+ and O_2^+ using polar plots in Fig. 6, we observe that for 7 fs the distributions are somewhat broader than for 40 fs. This is in agreement with the assertion that dynamic alignment has a strong influence on the angular distributions. For 40 fs the molecules have more time to align within the laser pulse, whereas for 7

fs this alignment is weaker. In addition, the comparison between the N_2^+ and O_2^+ angular distributions indicates that the (2,1) channel of O_2^+ for 7 fs is narrower than N_2^+ but for 40 fs the (2,1) channel of N_2^+ is narrower than O_2^+. Since N_2^+ is less massive, it shows a larger propensity to align.

Overall we find that the 7 fs data are also consistent with the stairstep mechanism used to explain the 40 fs data. Whereas for 40 fs the molecules stretch more between ionization steps, for 7 fs the molecules are not afforded this opportunity. Thus, in the limit of very long pulses ($\gtrsim 100$ fs) we expect that the stretching between steps will reach R values close to R_c, whereas in the limit of very short pulses (~ 3 fs or driven by electron rescattering) ionization will become more direct, occurring near $R = R_e$.

IV. SUMMARY

We have presented the results for the multiple ionization and fragmentation of the diatomic molecular ion beams N_2^+, CO^+, NO^+, and O_2^+, in intense laser pulses (40 and 7 fs) by applying a coincidence 3D momentum imaging method. This method allowed us to detect and distinguish the neutral from the ion fragments and hence clearly separate all fragmentation channels. In general, we find that, while for dissociation the KER and angular distributions are unique to a specific molecular ion, for higher ionization channels the spectra of all molecular ions under study start to resemble one another, the molecular ions seemingly losing their identity. We explain our observations on multiple ionization using a stairstep ionization mechanism that seems to be valid for both 40 and 7 fs pulses and that is similar to what has been proposed in earlier studies beginning with neutral molecule targets.

[1] C. Cornaggia, J. Lavancier, D. Normand, J. Morellec, P. Agostini, J. P. Chambaret, and A. Antonetti, Phys. Rev. A **44**, 4499 (1991).

[2] K. Codling and L. J. Frasinski, J. Phys. B **26**, 783 (1993) and references therein.

[3] J. H. Posthumus, Rep. Prog. Phys. **67**, 623 (2004).

[4] J. H. Posthumus, A. J. Giles, M. R. Thompson, and K. Codling, J. Phys. B **29**, 5811 (1996).

[5] S. Banerjee, G. R. Kumar, and D. Mathur, Phys. Rev. A **60**, R25 (1999).

[6] J. McKenna, M. Suresh, B. Srigengan, I. D. Williams, W. A. Bryan, E. M. L. English, S. L. Stebbings, W. R. Newell, I. C. E. Turcu, J. M. Smith, E. J. Divall, C. J. Hooker, A. J. Langley, and J. L. Collier, Phys. Rev. A **73**, 043401 (2006).

[7] W. Guo, J. Zhu, B. Wang, Y. Wang, and L. Wang, Phys. Rev. A **77**, 033415 (2008).

[8] F. Légaré, I. V. Litvinyuk, P. W. Dooley, F. Quéré, A. D. Bandrauk, D. M. Villeneuve, and P. B. Corkum, Phys. Rev. Lett. **91**, 093002 (2003).

[9] A. S. Alnaser, X. M. Tong, T. Osipov, S. Voss, C. M. Maharjan, P. Ranitovic, B. Ulrich, B. Shan, Z. Chang, C. D. Lin, and C. L. Cocke, Phys. Rev. Lett. **93**, 183202 (2004).

[10] P. B. Corkum, Phys. Rev. Lett. **71**, 1994 (1993).

[11] J. H. Posthumus, L. J. Frasinski, A. J. Giles, and K. Codling, J. Phys. B **28**, L349 (1995).

[12] T. Zuo and A. D. Bandrauk, Phys. Rev. A **52**, R2511 (1995).

[13] J. B. Greenwood, I. M. G. Johnston, P. McKenna, I. D. Williams, T. R. J. Goodworth, J. H. Sanderson, W. A. Bryan, A. A. A. El-Zein, W. R. Newell, A. J. Langley, and E. J. Divall, Phys. Rev. Lett. **88**, 233001 (2002).

[14] I. Ben-Itzhak, P. Q. Wang, J. F. Xia, A. M. Sayler, M. A. Smith, K. D. Carnes, and B. D. Esry, Phys. Rev. Lett. **95**, 073002 (2005).

[15] I. Ben-Itzhak, P. Q. Wang, J. F. Xia, A. M. Sayler, M. A. Smith, J. W. Maseberg, K. D. Carnes, and B. D. Esry, Nucl. Instrum. Methods Phys. Res. B **233**, 56 (2005).

[16] P. Q. Wang, A. M. Sayler, K. D. Carnes, J. F. Xia, M. A. Smith, B. D. Esry, and I. Ben-Itzhak, Phys. Rev. A **74**, 043411 (2006).

[17] H. Niikura, F. Légaré, R. Hasbani, A. D. Bandrauk, M. Yu. Ivanov, D. M. Villeneuve, and P. B. Corkum, Nature (London) **417**, 917 (2002).

[18] A. S. Alnaser, T. Osipov, E. P. Benis, A. Wech, B. Shan, C. L. Cocke, X.-M. Tong, and C. D. Lin, Phys. Rev. Lett. **91**, 163002 (2003).

[19] S. Chelkowski, A. Conjusteau, T. Zuo, and A. D. Bandrauk, Phys. Rev. A **54**, 3235 (1996).

[20] K. Codling, L. J. Frasinski, and P. A. Hatherly, J. Phys. B **21**, L433 (1988).

[21] H. Stapelfeldt, E. Constant, and P. B. Corkum, Phys. Rev. Lett. **74**, 3780 (1995).

[22] E. Baldit, S. Saugout, and C. Cornaggia, Phys. Rev. A **71**, 021403(R) (2005).

[23] J. H. Posthumus, J. Plumridge, M. K. Thomas, K. Codling, L. J. Frasinski, A. J. Langley, and P. F. Tadday, J. Phys. B **31**, L553 (1998).

[24] K. Miyazaki, T. Shimizu, and D. Normand, J. Phys. B **37**, 753 (2004).

[25] X. M. Tong, Z. X. Zhao, and C. D. Lin, Phys. Rev. A **66**, 033402 (2002).

[26] X. M. Tong, Z. X. Zhao, A. S. Alnaser, S. Voss, C. L. Cocke, and C. D. Lin, J. Phys. B **38**, 333 (2005).

[27] F. Anis, T. Cackowski, and B. D. Esry, J. Phys. B **42**, 091001 (2009).

[28] J. Wu, H. Zeng, J. Wang, and C. Guo, Phys. Rev. A **73**, 051402(R) (2006).

[29] J. P. Nibarger, S. V. Menon, and G. N. Gibson, Phys. Rev. A **63**, 053406 (2001).

[30] A. Talebpour, S. Larochelle, and S. L. Chin, J. Phys. B **30**, L245 (1997).

[31] L. J. Frasinski, K. Codling, and P. A. Hatherly, Science **246**, 1029 (1989).

[32] A. Iwamae, A. Hishikawa, and K. Yamanouchi, J. Phys. B **33**, 223 (2000).

[33] S. Voss, A. S. Alnaser, X.-M. Tong, C. Maharjan, P. Ranitovic, B. Ulrich, B. Shan, Z. Chang, C. D. Lin, and C. L. Cocke, J. Phys. B **37**, 4239 (2004).

[34] R. N. Coffee, L. Fang, and G. N. Gibson, Phys. Rev. A **73**, 043417 (2006).

[35] C. Cornaggia and L. Quaglia, Phys. Rev. A **63**, 030702(R) (2001).

[36] Ph. Hering and C. Cornaggia, Phys. Rev. A **57**, 4572 (1998).

[37] J. Wu, H. Zeng, and C. Guo, J. Phys. B **40**, 1095 (2007).

[38] H. Ren, R. Ma, J. Chen, X. Li, H. Yang, and Q. Gong, J. Phys. B **36**, 2179 (2003).

[39] C. Guo, Phys. Rev. A **71**, 021405(R) (2005).

[40] A. Talebpour, S. Larochelle, and S. L. Chin, J. Phys. B **30**, 1927 (1997).

[41] J. Wu, H. Zeng, and C. Guo, Phys. Rev. A **74**, 031404(R)

[42] H. Mashiko, C. M. Nakamura, C. Li, E. Moon, H. Wang, J. Tackett, and Z. Chang, Appl. Phys. Lett. **90**, 161114 (2007).

[43] D. J. Kane and R. Trebino, IEEE J. Quantum Electron. **29**, 571 (1993).

[44] P. Hansch and L. D. Van Woerkom, Opt. Lett. **21**, 1286 (1996).

[45] A. M. Sayler, P. Q. Wang, K. D. Carnes, and I. Ben-Itzhak, J. Phys. B **40**, 4367 (2007).

[46] B. Gaire, J. McKenna, A. M. Sayler, N. G. Johnson, E. Parke, K. D. Carnes, B. D. Esry, and I. Ben-Itzhak, Phys. Rev. A **78**, 033430 (2008).

[47] A. M. Sayler, P. Q. Wang, K. D. Carnes, B. D. Esry, and I. Ben-Itzhak, Phys. Rev. A **75**, 063420 (2007).

[48] A. Hishikawa, S. Liu, A. Iwasaki, and K. Yamanouchi, J. Chem. Phys. **114**, 9856 (2001).

[49] G. Handke, F. Tarantelli, and L. S. Cederbaum, Phys. Rev. Lett. **76**, 896 (1996).

[50] C. Jian-Xin and G. Qi-Huang, Chin. Phys. **14**, 1960 (2005).

[51] We note that increased alignment for higher ionization stages can also be explained by geometric alignment whereby the need for higher intensity selectively ionizes aligned molecules.

(2006).